

Binary Bosonic Mixtures with Pair Hopping in Synthetic Dimension: Phase Transitions and Demixing Effects

Chenrong Liu¹ and Zhi Lin^{2,3,*}

¹*College of Mathematics and Physics, Wenzhou University, Zhejiang 325035, China*

²*School of Physics and Optoelectronic Engineering, Anhui University, Hefei 230601, China*

³*State Key Laboratory of Surface Physics and Department of Physics, Fudan University, Shanghai 200433, China*

We employ the cluster Gutzwiller mean-field method to investigate the ground-state phase diagrams and demixing effects in binary boson mixtures with pair hopping in synthetic dimensions. Our study reveals two novel interspecies paired superfluid phases: the paired super-counter-fluid (PSCF) phase, featuring pairs of two particles of one species and two holes of the other, and the SCF* phase, which combines PSCF and super-counter-fluid (SCF) orders. These phases provide new insights into XY ferromagnet states from a pseudo-spin perspective, with SCF* and PSCF states corresponding to different XY ferromagnet phases depending on particle filling. We also identify a quantum quadruple critical point in the interexchange asymmetric case. Importantly, we demonstrate that the mixed-demixed critical point is phase-dependent due to pairing hopping, differing from normal two-component bosonic systems. Experimental schemes to observe these novel phases are proposed.

Ultracold atomic system in the optical lattice opens a new window to the research of modern condensed matter physics [1–4]. The remarkable control of the interactions between the atoms leads to the experimental realization of several interesting phase transitions in single-component bosonic systems, e.g., superfluid (SF) to Mott-insulator (MI) transition in a bosonic system with contact interaction [5] and superfluid-supersolid phase transition in a bosonic system with dipolar interaction [6–9]. Recently, more and more attention has been transferred from the single-component bosonic systems to the two-component bosonic systems thanks to the deepening of theoretical studies [10–12] and the progress of experimental methods [13–18]. One of the most significant experimental progress is the successful loading of two-component bosons into an optical lattice [13, 14, 18]. Notably, current achievements include the realization of the tunable Heisenberg model [15], tunable single-ion anisotropy in spin-1 models [16], observation of the spin-Mott state [17] and super-counterfluidity state (SCF) [18]. Theoretically, the physics of two-component bosons loaded into an optical lattice can be described by the traditional two-component Bose-Hubbard model (TCBH), which contains the intraspecies on-site interaction along with the interspecies on-site interaction, and gives rise to many new phases such as SCF, paired superfluid state (PSF), two-component Mott insulator phase (2MI), and two-component superfluid phase (2SF) [10, 12]. In these studies, the interexchange symmetry (a component \leftrightarrow b component) can be assumed, implying the same hopping amplitude and the same intraspecies on-site interaction for each species. By breaking this symmetry, the traditional TCBH model would have a more complex phase diagram.

Additionally, the systems of the two-component bosons

loaded into optical lattice are becoming a flexible platform for simulating the novel interspecies and intraspecies paired superfluid phases, i.e. SCF, PSF, and molecular superfluid (MSF) [10–12, 19–26]. It is interesting to explore whether the binary boson mixtures can exhibit new pairing phases. Twenty years ago, several seminal works [10, 11] point out that the so-called XY ferromagnet phase with XY order $\langle S^\dagger \rangle \neq 0$ can support the SCF phase. More generally, H. J. Schulz has uncovered that there exist two different types of XY ferromagnet phases in anisotropic Heisenberg spin- s chain ($s = 1/2, 1, 3/2, \dots$), which are XY1 phase with order $\langle (S^\dagger)^n \rangle \neq 0$ for all $n \leq 2s$ and XY2 phase with order $\langle (S^\dagger)^{2s} \rangle \neq 0$ (here $s > 1/2$) whereas $\langle (S^\dagger)^n \rangle = 0$ for all $n < 2s$ ($n = 1, 2, \dots$) [27]. With this definition, the SCF state is just the XY1 phase in quantum spin systems. Nevertheless, to the best of our knowledge, the bosonic phase related to the XY2 phase has not yet been studied. We can then further infer that the XY2 ferromagnet phase probably supports the new type of paired superfluid phase and this is one of the main motivations of this work.

On the other side, the synthetic dimensions as an effective tool have been widely used to simulate the particle motion along extra spatial directions [28–30]. With the help of synthetic dimensions, the higher-dimensional physics can be emulated in a lower-dimensional experimental platform [29]. Usually, time, momentum space, or internal states (the internal atomic degrees of freedom, e.g., pseudospin) can be considered as the synthetic dimensions [30, 31]. In contrast to manipulating the single-particle hopping processes [32–37], we have proposed a feasible scheme for handling two-particle hopping process along a synthetic dimension (or synthetic pair hopping) in a two-component bosonic system [26] via the Floquet engineering [38–41]. This synthetic pair hopping (SPH) interaction can be described as $(a_i b_i^\dagger)^2 + \text{H. c.}$, where a_i and b_i are the boson a and b annihilation operators on site

* Corresponding author; zhilin18@ahu.edu.cn

i. The SPH interaction may induce the order $\langle\langle ab^\dagger \rangle\rangle$, which is associate to the XY2 order $\langle\langle S^\dagger \rangle\rangle$. Therefore, although the TCBH+SPH model has been investigated in our previous work [26] without the interexchange symmetry, it is still worth to studying its phase diagram in detail.

Furthermore, a sufficiently strong interspecies repulsion can localize the two species in separated domains, and this leads to the broken of the spatial symmetry of the system. People have researched the critical condition of the spatial phase separation (demixing effect) in a traditional TCBH model, and they have shown that the mixed-demixed critical point is $U_{ab}/U = 1$, where $U_{ab} > 0$ is the repulsive interspecies on-site interaction and $U_{aa} = U_{bb} = U > 0$ is the repulsive intraspecies on-site interaction. Latter, people emphasized that the general demixing condition is $U_{ab}^2 > U_{aa}U_{bb}$ [42–46]. While it is still unknown how the demixing effect occurs when the SPH interaction is added to the traditional TCBH model. This is another motivation for the present work.

Results

The Model

The Hamiltonian of the two-component bosonic system with pair hopping in synthetic dimension can be read as [26],

$$\begin{aligned}
 H = & -J \sum_{\langle i,j \rangle} (a_i^\dagger a_j + b_i^\dagger b_j + \text{H. c.}) - \mu \sum_i (n_{i,a} + n_{i,b}) \\
 & + \frac{U_{aa}}{2} \sum_i n_{i,a} (n_{i,a} - 1) + \frac{U_{bb}}{2} \sum_i n_{i,b} (n_{i,b} - 1) \\
 & + U_{ab} \sum_i n_{i,a} n_{i,b} + W \sum_i (a_i^\dagger b_i a_i^\dagger b_i + \text{H. c.}), \quad (1)
 \end{aligned}$$

where a_i (b_i) is a (b) component boson annihilation operator and $n_{i,a}$ ($n_{i,b}$) is the corresponding number operator. We have proposed a feasible scheme for realizing this interesting Hamiltonian via the Floquet engineering [26], which has also been suggested in a multi-band Bose system [47, 48]. Here, the first five terms describe the traditional TCBH model [10, 12, 49] and the W term represents the SPH interaction. The interspecies interaction U_{ab} is repulsive ($U_{ab} > 0$). Moreover, the interexchange symmetry requests $U_{aa} = U_{bb}$, which can be broken by tuning these parameters. A sketch of this model in a two-dimensional square lattice is shown in Fig. 1, and the phase diagram for a typical interexchange asymmetric case is presented in our earlier work [26]. We investigate two novel phases: the non-integer Mott insulator (NMI) phase and molecular superfluid (MSF) phase. One of our main goals is to systematically survey the ground-state phase diagrams of these interesting two-component bosonic systems, regardless of whether the interexchange symmetry is broken.

The ground state phase diagram

To systematically study the influence of the pair hopping on the phase diagram of the traditional TCBH model(See Fig. A2 in Appendix. B1), we turn on the

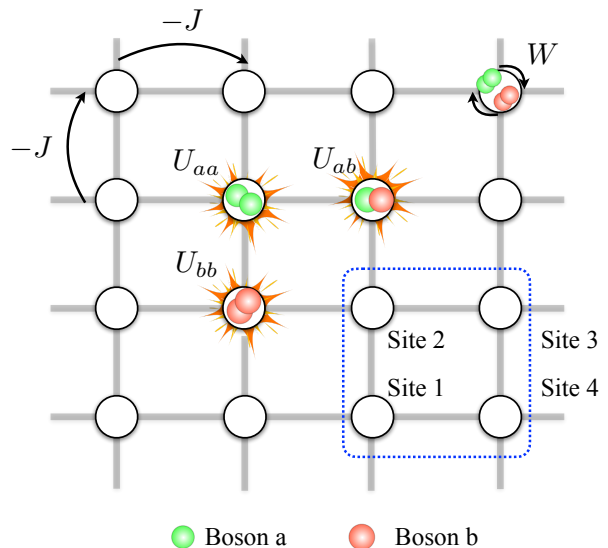


FIG. 1. (Color online) An illustration of the TCBH model with SPH in a two-dimensional square lattice. The dashed blue box indicates the unit cell used for the CGMF calculations. Each site inside the unit cell has been labeled by sites 1,2,3 and 4 for convenience.

W term, fixing its value at -0.1 (in units of U). We first consider the interexchange symmetric case, where $U_{aa} = U_{bb} = U$ is enabled. The phase diagram and the physical measurements are presented in Fig. 2(a)-(b). Interestingly, two new phases emerge: the paired SCF state (PSCF) and SCF*. In the PSCF phase, only the paired SCF order parameter $\langle\langle ab^\dagger \rangle\rangle$ is non-zero, while the other order parameters such as $\langle a \rangle$, $\langle b \rangle$, $\langle ab^\dagger \rangle_{J=0}$ and $\langle ab^\dagger \rangle_{J \neq 0}$ are all zero. These order parameters provide a straightforward understanding of the PSCF phases. In an SCF state (distinguished via the CGMF presented in Appendix. B2), the net atomic superfluid current is zero, but there exist equal superfluid currents of the components in opposite directions, each composed of single atoms [10]. Similarly, in the PSCF phase, the net atomic superfluid current is absent, and the equal single currents of two components in opposite directions are also forbidden. However, equal double currents of two species (each composed of two bound atoms of the same species) in opposite directions are superfluid. In other words, the PSCF phase can be viewed as the result of a pairing between two particles of one component and two holes of the other component. The W term facilitates this phase through pair-hopping between species. Importantly, the novel PSCF phase is supported by the XY2 phase, characterized by the order parameter $\langle\langle S^\dagger \rangle\rangle \neq 0$ when applying Schwinger boson transformation to map bosons onto spins.

On the other hand, the SCF* phase is characterized by non-zero values for both $\langle ab^\dagger \rangle$ and $\langle\langle ab^\dagger \rangle\rangle$, while all other order parameters remain zero. This indicates that the SCF* phase combines features of both the SCF and PSCF states, representing a novel paired superfluid phase

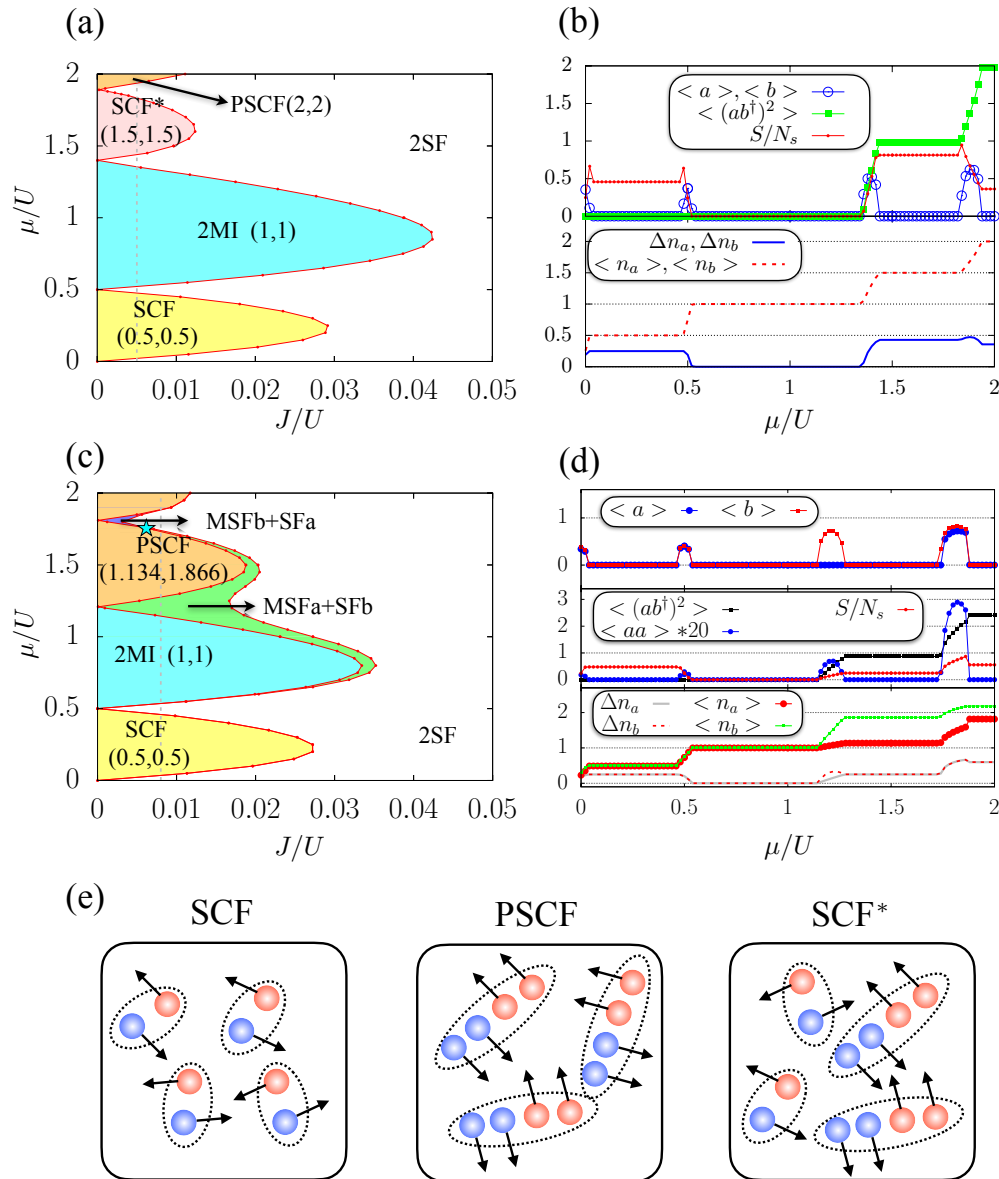


FIG. 2. (Color online) Chemical potential μ versus J phase diagram for (a) $U_{bb} = U_{aa} = U$ and (c) $U_{bb} = 0.8U_{aa} = 0.8U$. Here, $U_{ab} = 0.5U$ and $W = -0.1U$ are fixed. (b) and (d) are the measurements corresponding to the black dashed lines in (a) and (c) respectively, where J/U is fixed at 0.005 in (b) and is fixed at 0.008 in (d). In (a) and (c), the brackets (\cdot, \cdot) label the averaged particle numbers $(\langle n_a \rangle, \langle n_b \rangle)$ in the related phases. A star in (c) marks the quantum quadruple critical point. (e) A sketch of the SCF, PSCF, and SCF* phases. Different colors in the circles represent the different species, and the arrows label the moving direction of the bosons.

that has not been previously studied. If $W = 0$, then the SCF*(1.5,1.5) phase in Fig. 2(a) transitions to the normal SCF (1.5,1.5) state (See Fig. A2 in Appendix. B1). Thus, the existence of the SCF* phase is also attributed to the W term. A sketch of the SCF, PSCF, and SCF* phase has been shown in Fig. 2(e), with the behaviors of the order parameters summarized in Table. I.

Interestingly, unlike the SCF or 2SF phases, which request non-integer averaged single-component particle numbers, the PSCF phase can have integer filling for each

component $\langle n_\alpha \rangle$ ($\alpha = a, b$), such as $\langle n_a \rangle = \langle n_b \rangle = 2$ in Fig. 2 (a). This integer value arises from two constraints: a) The total particle number in the PSCF lobe is even (e.g. $\langle n_a \rangle + \langle n_b \rangle = 4$) and it is conserved; b) interexchange symmetry is preserved, i.e. requiring $\langle n_a \rangle = \langle n_b \rangle$. In addition, the averaged particle numbers in a PSCF lobe remain unchanged with increasing μ . These behaviors of averaged particle numbers are very similar to those of a 2MI state. However, the nonzero interspecies entanglement entropy S and the local particle number fluctua-

TABLE I. Identification of SCF, PSCF, and SCF* phases in terms of the values of order parameters $\langle\alpha\rangle$ ($\alpha = a, b$), $\langle ab^\dagger\rangle_{J=0}$, $\langle(ab^\dagger)^2\rangle$, interspecies entanglement entropy S , and single-component particle number fluctuations $\Delta n_{a/b}$. Reminder that all these observables are calculated based on the CGMF ground states and have been averaged by the size of the cluster.

Phases	$\langle\alpha\rangle$	$\langle ab^\dagger\rangle_{J=0}$	$\langle ab^\dagger\rangle_{J\neq 0}$	$\langle(ab^\dagger)^2\rangle$	S	$\Delta n_{a/b}$
SCF	0	$\neq 0$	0	0	$\neq 0$	$\neq 0$
PSCF	0	0	0	$\neq 0$	$\neq 0$	$\neq 0$
SCF*	0	$\neq 0$	0	$\neq 0$	$\neq 0$	$\neq 0$

tions Δn_α ($\alpha = a, b$) reveal that the PSCF phase is both interspecies entangled and compressible, distinguishing it from the 2MI phase, consistent with the order parameter conclusions.

We now explore the effects of breaking interexchange symmetry by tuning $U_{bb} = 0.8U < U_{aa} = U$. The results, presented in Figs. 2(c)-(d), reveal that the PSCF phase still exists, but its averaged single-component particle number $\langle n_\alpha\rangle$ ($\alpha = a, b$) becomes non-integer. This is different with the symmetric case, where the value of $\langle n_\alpha\rangle$ ($\alpha = a, b$) is an integer. The reason is that although $f = \langle n_a\rangle + \langle n_b\rangle$ is a conserved integer, $\langle n_a\rangle$ and $\langle n_b\rangle$ must be unequal in the asymmetric case, and their values depend on the imbalance of U_{aa} and U_{bb} . Thus, the PSCF phase in this scenario corresponds to non-integer Mott insulator (NMI) state mentioned in our previous work [26]. However, the PSCF order parameter $\langle(ab^\dagger)^2\rangle$ has not yet been evaluated in that study.

The MSFa and MSFb phases, alongside the SCF* and the PSCF phase, are also observed in Fig. 2(c). Notably, we identify a quantum quadruple critical point (marked by stars) in Fig. 2(c). Additionally, several quantum quadruple critical points appear in system with small value of $U_{ab} = 0.1U$ (See Fig. A4 (h) in Appendix. C). This novel quantum quadruple critical point represents a phase transition among the 2SF, PSCF, MSFa+SFb, and MSFb+SFa. To the best of our knowledge, it the first instance of a quantum quadruple critical point being revealed in a TCBH+SPH model. The MSFa and MSFb are similar, as they represent molecular superfluids of species a and b , respectively. Here, we mainly discuss the properties of MSFa. As shown in Fig. 2(d), the MSFa state exhibits a non-zero molecular SF order for boson a ($\langle aa\rangle \neq 0$) and zero atomic SF order for boson a ($\langle a\rangle = 0$). This means that in the MSFa phase, two atoms of boson a are paired to form an SF state, while the a atoms themselves are in an MI state. The origin of the MSFa+ SFb phase can be easily understood within the framework of mean-field theory. In the absence of the W term, consider the system in the SFb+MIa phase. An operator can be replaced by its corresponding SF order parameter in an SF state within mean-field theory. After the SPH is added, the W term can be rewritten using the SF order parameter of boson b and it is $a_i^2(\psi_i^*)^2 + H.c.$,

where $\psi_i^* = \langle b_i^\dagger\rangle$. Consequently, the W term is simplified as $a_i^2 + H.c.$, which leads to a non-zero molecular SF order of boson a , while the atomic SF order of boson a remains zero owing to the system is in MIa phase. Thus, the SFb+MIa phase transitions to the SFb+MSFa phase with the introduction of the W term. As mentioned in Appendix. B1, the SFb+MIa requests the breaking of the interexchange symmetry, suggesting that the MSFa phase does not exist in the symmetric case, consistent with our numerical results (see Fig.2(a)) and effective-field analysis from our previous work [26]. However, if U_{ab} reaches a specific (critical) value U_{ab}^c , as illustrated in Fig. A4(e), the MSFa phase unexpectedly vanishes in asymmetric cases.

Moreover, the interspecies interaction U_{ab} can significantly influence the phase diagram. For example, the second lobe in Fig. 2(a) is labeled as the 2MI phase at $U_{ab}/U = 0.5$, but we will demonstrate that this is not always the case, as the phase can be 2MI, SCF*, or PSCF depending on the value of U_{ab} (See details in Appendix. C). At the atomic limit ($J = 0$), we theoretically analyze the second lobe's ground state and identify a critical value of U_{ab} , given by $U_{ab}^c = U_{bb} + 2Wk$, where k is a parameter. For $U_{ab} < U_{ab}^c$, the second lobe corresponds to the 2MI phase, whereas for $U_{ab} > U_{ab}^c$, it transitions to a PSCF state. In particular, at $U_{ab} = U_{ab}^c$, the lobe can exhibit an SCF* phase, regardless of whether the system is interexchange symmetric or asymmetric. In addition, the chemical potential width $\Delta\mu$ of the first SCF lobe at $J = 0$ in Figs. A4 also expands as U_{ab} increases until it reaches U_{ab}^c , specifically, $\Delta\mu = U_{ab}(U_{ab}^c)$ for $U_{ab} \leq U_{ab}^c$ ($U_{ab} > U_{ab}^c$) (details in Appendix. C).

Mixed-demixed phase transition

If a strong interspecies interaction is tuned, it can induce a demixing effect, leading to phase separation (or collapse) and system instability. Next, we will examine how the above phases evolved in a demixed phase when U_{ab} is sufficiently large, focusing on the interexchange symmetric case where $U_{aa} = U_{bb} = U$ is fixed. In a mixed phase, $\langle n_a\rangle = \langle n_b\rangle$ holds true across all phases. However, in a completed demixed phase, the two species can not coexist on a single site, resulting in $\langle n_a\rangle \neq \langle n_b\rangle$, which breaks the interexchange symmetry spontaneously. To illustrate this, we present $\langle n_a\rangle$ and $\langle n_b\rangle$ as functions of U_{ab} in Fig. 3.

At $W = 0$, it is known that two species mix well when the condition $U_{ab}^2 < U_{aa}U_{bb}$ is satisfied, with $U_{aa} > 0$ and $U_{bb} > 0$ being repulsive [42]. Consequently, the traditional two-component bosonic system would undergo a phase transition to the demixed state with a critical point $U_{ab}^c = U$ [43–46] in the interexchange symmetric case. We reproduce this result in Fig. 3(a). Starting with $U_{ab} = 0.5U$, we set (J, μ) point in 2MI, SCF, and 2SF phases. By increasing U_{ab} in Fig. 3(a), the mixing-demixing transition is observed across all phases, and the critical points $U_{ab}^c = U$ are independent of the quantum phases, consistent with the previous studies.

For the $W/U = -0.1$ case, the pair-hopping term

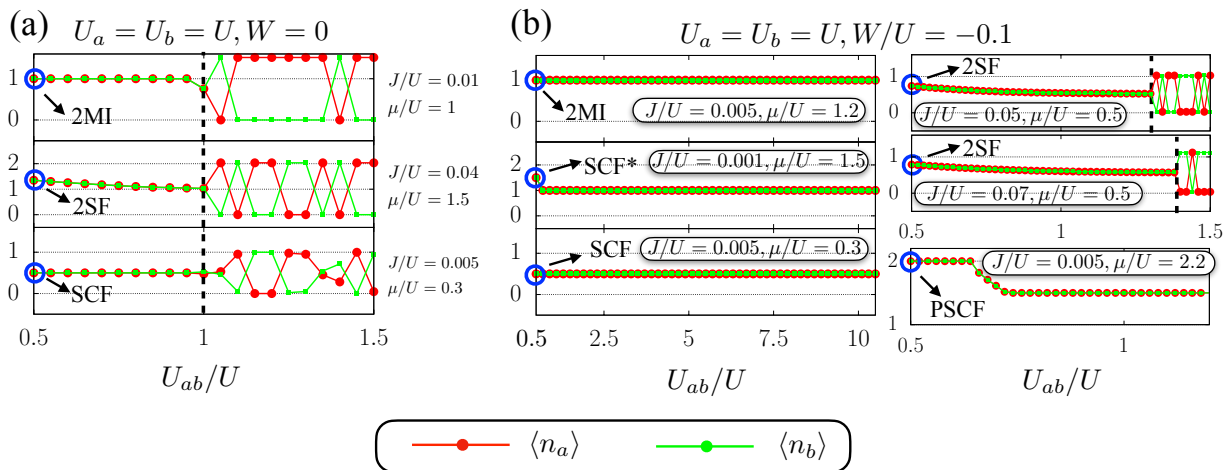


FIG. 3. (Color online) Demixing effect at (a) $W = 0$ and (b) $W/U = -0.1$ with the interexchange symmetry is preserved. Here, we start tuning the U_{ab} from 0.5 which is set in Figs. A2 and 2, and all the other model parameters are fixed. The black dashed vertical lines mark the mixing-demixing phase transition points. The labeled quantum phases at $U_{ab}/U = 0.5$ are the same as that in Figs. A2 and 2.

would affect the mixed-demixed phase transition point. The W term reduces total energy through double opposite hopping between species, favoring a mixed state. The hopping strength is highly dependent on the particle numbers, i.e., larger particle numbers enhance hopping. As a result, the mixed-demixed phase transition point U_{ab}^c becomes phase-dependent when the W term is introduced. To check it, we start with different phases at $U_{ab}/U = 0.5$, and examine their evolution as we increase U_{ab} . As shown in Fig. 3 (b), we initially set (J, μ) in 2MI, 2SF, SCF, PSCF, and SCF* phases at $U_{ab}/U = 0.5$. Interestingly, only the 2SF phase exhibits a demixing phase transition, while other phases remain mixed even at high U_{ab} . This differs from the situation in Fig. 3 (a). Moreover, the mixing-demixing critical point in the 2SF phase depends on the parameters. Based on these numerical results, we first emphasize that the mixed-demixed phase transition point is indeed dependent on the initial phases when the W term exists.

Experimental detection

The TCBH+SPH model has been proposed in two different schemes: one involves our previous Floquet engineering scheme, which also discusses the uncontrollable heating from time-periodic driving [26], while the other is based on a multi-band Bose system [47, 48]. Although the SCF has recently been observed experimentally through antipair correlations measurements [18], the other three phases, MSFa, PSCF, and SCF*, have yet to be detected. Thus, we will introduce feasible experimental schemes for observing these three novel paired superfluid phases.

In our previous works [26], we demonstrated that the SFb+MSFa phase can be directly detected by spin-resolved time-of-flight (TOF) images. However, the Bose-Einstein condensation peak of the MSFa phase ap-

pears only in the momentum molecular density distribution, necessitating the application of Feshbach resonance to project atoms of component a onto the Feshbach molecules aa , preceded by spin-resolved TOF images, which complicates the experimental process. Notably, the strong antipairing correlations ($k = k'$) in noise correlation functions of the interspecies bosons, defined as $G_{a,b} = \langle n_{a,k} n_{b,k'} \rangle - \langle n_{a,k} \rangle \langle n_{b,k'} \rangle$, serve as a signature for detecting SCF phase [18, 50]. We highlight that antipairing along $k = k'$ and pairing correlations along $k = -k'$ in the intraspecies correlation function $G_{a,a}$ uniquely characterize the MSFa phase. Here, k, k' are momenta, while $n_{a,k}$ and $n_{b,k}$ are the occupation operators in momentum space.

To characterize the MSFa+SFb phase, we calculate $G_{a/b,a/b}$ and $G_{a,b}$ in a one-dimensional chain with periodic boundary conditions using the density matrix renormalization group (DMRG) algorithm implemented in the ITensor Library [51]. The maximum single-component boson occupancy per site is fixed at 5. In DMRG calculations, we kept up to 1800 states for each sweep, with a maximum of 100 sweeps. DMRG precision is validated by examining the total energy variance, set to be 10^{-10} . For a lattice size $L = 32$, the actual number of sweeps is 20~30, and the truncation error is up to 10^{-10} . The results are presented in Fig. 4.

In Fig. 4(a), the logarithmic plot of the correlation functions reveals the power-law decay of $\langle b_i^\dagger b_j \rangle$ and $\langle (a_i^\dagger)^2 (a_j)^2 \rangle$, alongside the exponential decay of $\langle a_i^\dagger a_j \rangle$, indicating that the system is in the MSFa+SFb phase. Strictly speaking, this superfluid phase in one dimension is a Luttinger liquid of molecular a and atom b . The signature of this phase in the noise correlation functions can be found in Figs. 4(b)-(d). As shown in Fig. 4(b), $G_{a,a}$ exhibits strong antipairing along $k = k'$ and pair-

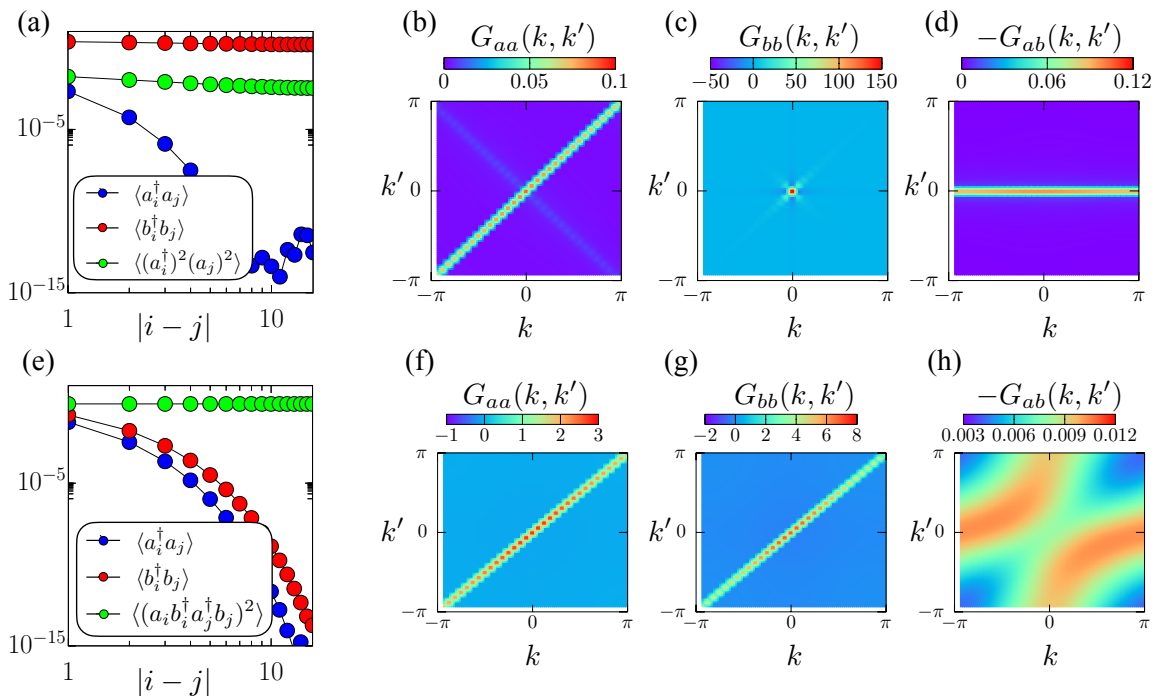


FIG. 4. (Color online) DMRG calculations for MSFa phase ((a)-(d)) and PSCF phase ((e)-(h)) of a one-dimensional TCBH chain with SPH are presented. Panels (a) and (e) show the correlation functions, while (b)-(d) and (f)-(h) display the noise correlation functions. The size of the chain is $L = 32$, with fixed parameters $U_{ab}/U_{aa} = 0.5$ and $W/U_{aa} = -0.1$. The model parameters are set as $J/U_{aa} = 0.02$, $U_{bb}/U_{aa} = 0.1$ for (a)-(d) and $J/U_{aa} = 0.01$, $U_{bb}/U_{aa} = 0.8$ for (e)-(h). Using the canonical ensemble Hamiltonian, the total particle filling factor is fixed at $(N_a + N_b)/L = 3$, where N_a and N_b are the total particle number of a and b species, respectively. Note that N_a and N_b are not conserved numbers owing to the W term, but the total particle number $N = N_a + N_b$ is conserved.

ing correlations along $k = -k'$, reflecting the MI feature [50] and the formation of pairing of two bosons of component a , respectively. In Fig. 4(c), the peaks of $G_{b,b}$ are primarily at $k = k' = 0$, indicating the SF state of b species [50]. For $G_{a,b}$ in Fig. 4(d), the peaks along the $k' = 0$ direction suggest that boson b is condensed at $k' = 0$ while boson a remains in a MI state. More importantly, Fig. 4(d) also shows the absence of interspecies antipairing or pairing. These noise correlation features align with the correlation functions in Fig. 4(a). Recent experiments have measured the noise correlation function $G_{a,b}$ in a binary Bose mixture trapped in optical lattices, suggesting that characteristics of the MSFa phase can be explored using the same experimental techniques.

The noise correlation functions discussed above can also be used as a probe for the PSCF phase. The related DMRG calculations are shown in Figs. 4(e)-(h). In Fig. 4(e), the features of the correlation functions $\langle a_i^\dagger a_j \rangle$, $\langle b_i^\dagger b_j \rangle$ and $\langle (a_i^\dagger b_i^\dagger a_j b_j)^2 \rangle$ indicate that the phase is the PSCF phase. Since there is no long-range single species SF order, the peaks of $G_{a,a}$ and $G_{b,b}$ in Figs. 4(f)-(g) are located along the $k = k'$ direction, which indicates a Mott feature of boson a and boson b . Intriguingly, as illustrated in Fig. 4(h), the positions of the $G_{a,b}$ peaks form two arcs along $(-\pi, 0) \rightarrow (0, \pi)$ and $(0, -\pi) \rightarrow (\pi, 0)$.

This behavior of $G_{a,b}$ differs from that of the SCF phase reported in Ref. [50] and can be regarded as a distinguishing characteristic of the PSCF in experiments.

On the other hand, the pairing features of the PSCF phase can be revealed by combining noise correlation methods with Feshbach resonance techniques. Specifically, consider a binary Bose mixture in which single-species Feshbach molecules (i.e., molecule aa and molecule bb) are formed when both species are subjected to the same magnetic field. Then, after making a fast ramp across a Feshbach resonance, the strong antipairing correlations in the noise correlation function of molecules aa and bb , expressed as $F_{a,b} = \langle M_{a,k} M_{b,k'} \rangle - \langle M_{a,k} \rangle \langle M_{b,k'} \rangle$, would be detected if the mixture is in a PSCF phase. Here, $M_{a/b,k}$ is the operator of the Feshbach molecule aa/bb , which is in contrast to $G_{a,b}$. Similar to the SCF phase, if all the peaks of $F_{a,b}$ are located along the $k = k'$ direction, we can immediately infer that the $aab^\dagger b^\dagger$ pairing is formed, indicating a PSCF state.

In practice, there is a feasible way to recognize the PSCF phase in experiments based on the above discussions. From the Fig. 1 of Ref. [52], we find there are two types of Feshbach molecules $^{87}\text{Rb}_2$, corresponding to the states $(f_1 = 1, f_2 = 1)\nu = -2$ (where ν is a vibrational quantum number) and $(f_1 = 1, f_2 = 2)\nu = -4$, can be constructed respectively via Feshbach resonances

in the entrance channels $|f = 1, m_f = 1\rangle \otimes |1, 1\rangle$ and $|1, 0\rangle \otimes |1, 0\rangle$, with a magnetic field of approximately $410G$ [52]. Thus, if we choose the binary ^{87}Rb mixture with states $|f = 1, m_f = 1\rangle$ and $|f = 1, m_f = 0\rangle$, it is optimistic to expect the possibilities of observing this novel PSCF phase when the SPH is included. This scheme can be used in the observation of the SCF* phase. Since the SCF* phase supports both the PSCF and SCF orders, it can be detected using a combined approach that integrates measurements from both the SCF and PSCF phases.

Discussion

In this work, we have systematically studied the ground-state phase diagram of the traditional TCBH model with SPH interaction using the CGMF method. Interestingly, we have revealed two new phases: PSCF and SCF*. Moreover, we have also demonstrated that these two phases can be re-interpreted as a new type of XY ferromagnet phase from the perspective of pseudospins. According to H. J. Schulz's work [27], the XY ferromagnet phase in a spin- s ($s = 1/2, 1, \dots$) system can be divided into two types: XY1 and XY2. In the XY1 phase, the transverse spin order $\langle (S^\dagger)^n \rangle \neq 0$ for all $n \leq 2s$, while in the XY2 phase, only $\langle (S^\dagger)^{2s} \rangle \neq 0$ and $\langle (S^\dagger)^n \rangle = 0$ for all $n < 2s$, where $n = 1, 2, \dots, 2s$ is an integer. As pointed out in Refs. [10, 53], different spins can be simulated based on the filling factor (averaged particle numbers $\langle n_{a/b} \rangle$) of the two species, with the relation $s = (\langle n_a \rangle + \langle n_b \rangle)/2 = f/2$, where $f = \langle n_a \rangle + \langle n_b \rangle$ denotes the total averaged particle number. The PSCF phases with different total averaged particle numbers can be reconsidered as different types of XY ferromagnet phase. For instance, the PSCF phases with $f = 2$ in Figs. A4(c) and (f) relate to a spin-1 XY2 phase with orders $\langle (S^\dagger)^2 \rangle \neq 0$ and $\langle S^\dagger \rangle = 0$. Whereas for other PSCF lobes, e.g. PSCF(2,2) and PSCF(1.134,1.866) in Fig. 2, represent a new type of XY ferromagnet characterized by $\langle (S^\dagger)^2 \rangle \neq 0$ and $\langle S^\dagger \rangle = \langle (S^\dagger)^3 \rangle = \langle (S^\dagger)^4 \rangle = 0$, as they do not satisfy the criteria for the XY1 or XY2 phase [27]. Similarly, the SCF* phases in Figs. A4(b) and (e) with $f = 2$ correspond to a spin-1 XY1 phase, but the SCF* phase shown in Fig. 2(a) with $f = 3$ is associated with a new type of XY ferromagnet, as its orders satisfy $\langle S^\dagger \rangle \neq 0$, $\langle (S^\dagger)^2 \rangle \neq 0$ and $\langle (S^\dagger)^3 \rangle = 0$.

Additionally, we have discovered that the regions of two interspecies paired superfluid phases (PSCF and SCF*) in the ground-state phase diagram can be affected by the strength of the interspecies interaction U_{ab} . More interestingly, we have identified a quantum quadruple critical point in this binary boson mixture at small U_{ab} , marking the first time such a critical point has been revealed in a TCBH+SPH model.

Furthermore, we have uncovered the influence of the demixing effect on the phase diagram for the two-component bosonic system with SPH interaction. If U_{ab} is too strong, demixing occurs only in the 2SF phase, while other phases remain mixed. This indicates that the mixing-demixing critical point depends on the spe-

cific phase present at finite W , in contrast to the behavior observed in the traditional TCBH model, where all phases are unstable and transition to demixed states at the same critical point. Finally, we propose experimental schemes to observe other novel paired superfluid phases, i.e., MSFa, PSCF, and SCF* states, demonstrating that these phases can be detected by measuring antipairing (or pairing) correlations in the noise correlation function.

Methods

The cluster Gutzwiller mean-field method

To study the ground-state phase diagrams of Hamiltonian (1), we employ the CGMF [54–57], which effectively captures the quantum fluctuations in short range. The CGMF is particularly suitable for the two-dimensional two-component interacting bosonic systems due to the high degree of freedom at a single site, which is challenging for other numerical methods. The details about this method can be found in Refs. [55, 57] and we summarize key points of our CGMF calculations in the following.

Here, we use a 2×2 cluster, which is indicated by the blue dashed box in Fig. 1, as the unit cell. In the CGMF, the single-component boson occupation number cutoff N^c is an crucial parameter, as a value that is too small can significantly affect the results. To find a suitable N^c , we have tested some values of N^c in Appendix A and find that $N^c = 5$ is sufficient for $\mu/U < 2$. Another important parameter in the CGMF is the converge precision η . We set η to 10^{-8} with the convergence condition $\Delta < \eta$, where Δ is defined as $\Delta = |E_\ell - E_{\ell-1}| + \sum_{i \in \square, \alpha=a,b} |\langle \alpha_i \rangle_\ell - \langle \alpha_i \rangle_{\ell-1}|$, which is the energy and order parameter difference between two continuous self-consistent steps ℓ and $\ell - 1$. The label $i \in \square$ represents a summation in the unit cell. Thus, both the energy and single component SF order parameter converge upon completion of the self-consistent process.

To identify quantum phases, we calculate the related order parameters $\langle \alpha \rangle$ ($\alpha = a, b$), $\langle aa \rangle$, $\langle ab^\dagger \rangle$ and $\langle (ab^\dagger)^2 \rangle$, along with the single-component particle numbers $\langle n_\alpha \rangle$. Additionally, we evaluate the single-component particle number fluctuations Δn_α and the interspecies entanglement entropy S . All measurements are averaged over the unit cell lattice size, e.g. $\langle a \rangle = \frac{1}{4} \sum_{i \in \square} \langle a_i \rangle$.

We define the single-component particle number fluctuations as $\Delta n_\alpha = \frac{1}{4} \sum_{i \in \square} \langle \Delta n_{\alpha,i} \rangle = \frac{1}{4} \sum_{i \in \square} (\langle n_{\alpha,i}^2 \rangle - \langle n_{\alpha,i} \rangle^2)$, which helps identify whether a quantum phase of boson α is compressible [58, 59]. A phase is incompressible (compressible), if $\Delta n_{\alpha,i}$ is zero (non-zero) at all sites. Additionally, we extract S from the cluster ground state to classify the interspecies pairing phase [57]. S is calculated by tracing out the degrees of freedom of boson b , yielding the reduced density matrix of boson a : $\rho_a = \text{Tr}_b \rho = \text{Tr}_b |\Psi\rangle\langle\Psi|$, where $|\Psi\rangle$ is the CGMF ground state expressed as a linear combination of the many-body Fock states $|m_1^a, \dots, m_4^a; m_1^b, \dots, m_4^b\rangle$ (with m_i^α being the occupation number of boson α on site i). Finally, S is given by $S = -\sum_j \lambda_j \ln \lambda_j$, where λ_j is the j -th eigenvalue of ρ_a . A more efficient numerical method to

evaluate S is thought the Schmidt decomposition of $|\Psi\rangle$ over the two species [57].

Data available

Data analysis and simulation codes are available upon reasonable request.

Acknowledgements

The authors thank Y. Chen and J. Lou for fruitful discussions. This research is supported by the National Natural Science Foundation of China (NSFC) under Grant No.12004005, the Scientific Research Fund for Distinguished Young Scholars of the Education Department of Anhui Province No.2022AH020008, the Natural Science Foundation of Anhui Province under Grant No. 2008085QA26, the Scientific Research Fund of Zhejiang Provincial Education Department under Grant No. Y202248878, the Ph.D. research Startup Foundation of Wenzhou University under Grant No. KZ214001P05, and the open project of the state key laboratory of surface physics in Fudan University (Grant No. KF2021_08 and Grant No. KF2022_06).

Appendix A: Determining the suitable choice of N^c

To determine the value of the boson cutoff N^c , we plot $\langle a \rangle$ as a function of μ/U for different choices in Fig. A1. As it shows, $N^c = 5$ is good enough for $\mu/U < 2$. To improve the computational efficiency, an alternately setting of N^c can be employed, e.g. $N^c = 2, 3, 4$, and 5 when μ/U is in the regions $(0, 0.5]$, $(0.5, 1]$, $(1, 1.5]$, and $(1.5, 2]$ respectively. Under these settings, the mean-field Hamiltonian matrix dimension is up to $D = [(N^c + 1)^2]^4 = [(5 + 1)^2]^4 = 1679616$.

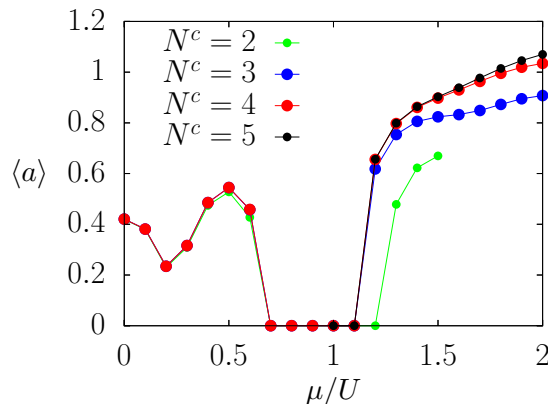


FIG. A1. (Color online) Test of the boson maximum occupancy number cutoff. The model parameters are set as $U_{aa} = U_{bb} = U$, $U_{ab}/U = 0.5$, $W/U = -0.1$, and $J/U = 0.03$.

Appendix B: Ground state properties for the traditional TCBH model $W = 0$

1. Ground-state phase diagram

The ground-state phase diagram of the traditional TCBH model ($W = 0$) has been widely studied in two dimensions [42, 60, 61]. For the interexchange symmetric case, there are three phases, namely 2SF, SCF, and 2MI exist in the phase diagram. In Fig. A2(a), we reproduce this result by setting $U_{aa} = U_{bb} = U$ (U is the energy unit). At $J = 0$, the chemical potential widths of the two SCF lobes are the same and equal to $0.5U$. The two SCF lobes are separated from each other by a 2MI lobe with a chemical potential width U at $J = 0$. All these calculations are exactly consistent with the previous works [61, 62].

To locate the 2MI-2SF phase boundaries, people usually use the value of the SF orders $\langle a \rangle$ and $\langle b \rangle$. For instance, in a 2SF state, $\langle a \rangle \neq 0$ and $\langle b \rangle \neq 0$, but they are both equal to zero in the 2MI phase. The SCF-2SF phase boundaries can be obtained using the same way because the SCF phase is such a state in which the order parameter $\langle ab^\dagger \rangle$ is non-zero, while $\langle a \rangle$ and $\langle b \rangle$ are both equal to zero within the mean-field theory. However, in the actual CGMF calculations, the onsite order parameter $\langle ab^\dagger \rangle_{J \neq 0}$ is always zero for the SCF phase (See details in Sec. B2). The SCF-2SF phase boundaries are therefore also determined using $\langle a \rangle$ and $\langle b \rangle$. It should be reminded here that the SCF phase is not an MI state although they both have a vanished SF order. To illustrate this, the interspecies entanglement entropy S and the particle number fluctuations Δn_α ($\alpha = a, b$) are evaluated. All these quantities as well as the averaged particle numbers as a function of μ are presented in Fig. A2(b) for a fixed value of J .

From Fig. A2(b), we can learn that the averaged particle numbers $\langle n_a \rangle$ and $\langle n_b \rangle$ do not change with increasing chemical potential μ in the 2MI lobe. This can be described by $\partial \langle n_{a/b} \rangle / \partial \mu = 0$, making the 2MI phase is incompressible [63]. Nevertheless, the criterion of $\partial \langle n_{a/b} \rangle / \partial \mu = 0$ is not always reliable for determining incompressibility in two-component bosonic systems. For example, in the SCF phase, $\partial \langle n_{a/b} \rangle / \partial \mu$ is also zero, but the phase is compressible because its particle number fluctuations $\Delta n_{a/b}$ shown in Fig. A2(b) are nonzero [58, 59]. Accordingly, a phase is considered incompressible if $\Delta n_{a/b} = 0$ in this paper. Besides, one can also find that the SCF phase is an entangled state due to the non-zero values of S , in contrast to the disentangled 2MI phase. These characteristics indicate that the CGMF method can well capture the superfluid properties of the SCF phase.

On the other hand, a more complex phase diagram is observed when the interexchange symmetry is broken. We recall here that we break the interexchange symmetry manually by setting $U_{bb} = 0.8U \neq U_{aa} = U$. As shown in Fig. A2(c), there are two new phases compared

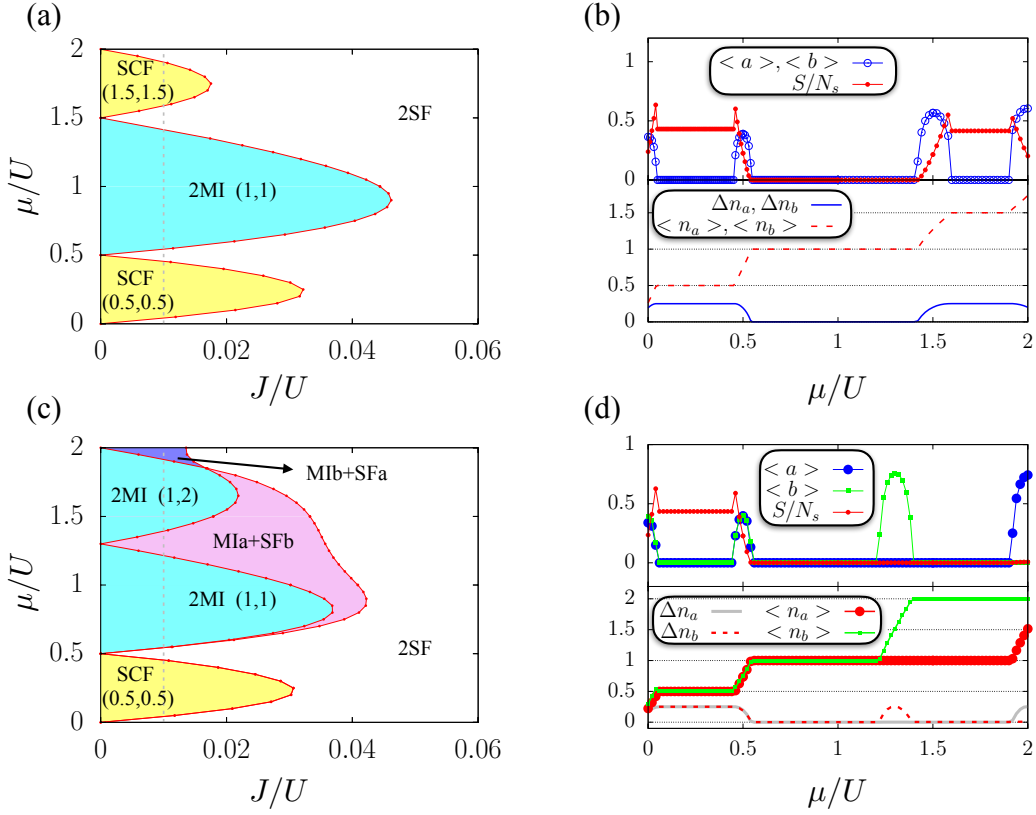


FIG. A2. (Color online) Chemical potential μ versus J phase diagram for (a) $U_{bb} = U_{aa} = U$ and (c) $U_{bb} = 0.8U_{aa} = 0.8U$, here U_{ab} is fixed at $0.5U$ and $W = 0$. (b) and (d) are the measurements corresponding to the black dashed lines in (a) and (c) respectively. In (a) and (c), the symbols (...) label the single-component averaged particle number ($\langle n_a \rangle$, $\langle n_b \rangle$). In (b) and (d), $N_s = 4$ is the number of sites in the cluster.

with Fig. A2(a), namely SFb+MIa and SFa+MIB. In the SFb+MIa (SFa+MIB) phase, b (a) component bosons are in an SF state while a (b) component bosons form a MI state. As displayed in Fig. A2(d), the two new phases are interspecies disentangled which leads to $S = 0$. For this reason, bosons a and b are decoupled in the two new phases. Other measurements can be also viewed in Fig. A2(d) and it is compatible with the phase diagram in Fig. A2(c).

More importantly, the regions of the SCF phase in Fig. A2(c) are dramatically shrunk compared to that in Fig. A2(a). For example, there are two SCF lobes shown in Fig. A2(a), while only the first SCF lobe is left in Fig. A2(c). In fact, all these SCF lobes with $\langle n_{a/b} \rangle \geq 1.5$ are vanish when the interexchange symmetry is broken. In other words, it implies that the prospects of observing an SCF phase in the interexchange symmetric case are much higher than in the interexchange asymmetric case.

This phenomenon can be understood in the following. At $J = 0$, the ground state of the whole system $|\Psi\rangle_{J=0}$ can be decoupled as the product of the single-site states, $|\Psi\rangle_{J=0} = \otimes_i |\psi\rangle_i$, i is the site index. For the SCF(1.5,1.5) phase, $|\psi\rangle_i = \sum c_{m_a, m_b} |m_a, m_b\rangle = (|1, 2\rangle + |2, 1\rangle)/\sqrt{2}$ where $|1, 2\rangle$ and $|2, 1\rangle$ are the two degenerate Fock states. But if the interexchange symmetry is broken, $|1, 2\rangle$ and

$|2, 1\rangle$ are no longer degenerate and the former has the lower energy since $U_{bb} < U_{aa}$. This means that $|\psi\rangle_i$ is $|1, 2\rangle$ rather than a superposition, and it represents the ground state of the 2MI(1,2) phase shown in Fig. A2(c). As a result, the SCF(1.5,1.5) lobe of Fig. A2(a) is replaced by the 2MI(1,2) lobe of Fig. A2(c). This explanation can be generalized to the disappearance of other SCF lobes with $\langle n_{a/b} \rangle > 1.5$. For the SCF(0.5,0.5) lobe, $|\psi\rangle_i = (|1, 0\rangle + |0, 1\rangle)/\sqrt{2}$. The SCF(0.5,0.5) state is special because $|1, 0\rangle$ and $|0, 1\rangle$ remain degenerate regardless of whether the interexchange symmetry is present. That is why the SCF(0.5,0.5) lobe can exist in both Fig. A2(a) and (c). From the perspective of the effective spin model, the SCF(0.5,0.5) and 2MI(1,2) phases correspond to the XY ferromagnet and the $S^z = (\langle n_a \rangle - \langle n_b \rangle)/2 = -1/2$ phases respectively as discussed in Ref. [11]. Our result in Fig. A2(c) is in agreement with the previous theoretical analysis.

2. Distinguishing the SCF state via the CGMF

In this part, we primarily discuss how we recognize the SCF phase using the CGMF method. The SCF phase can be treated as a paired superfluid phase where the inter-

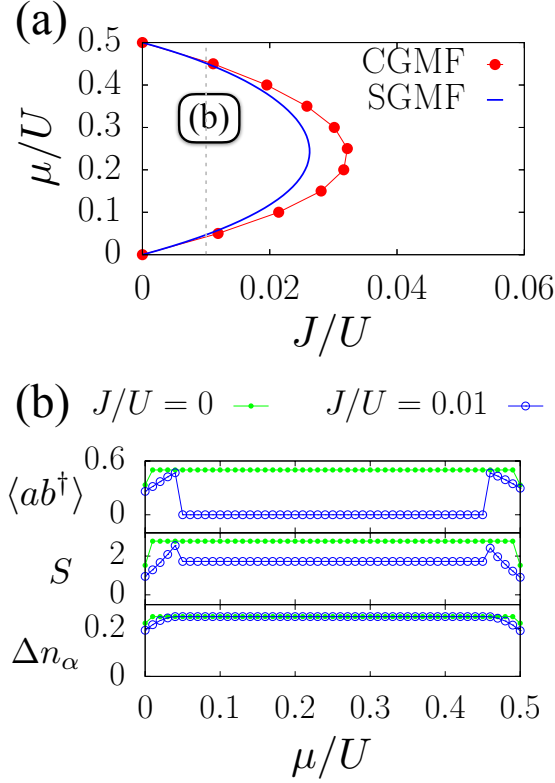


FIG. A3. (Color online) (a) SCF phase boundaries obtained using the SGMF and CGMF. (b) The CGMF measurements correspond to the black dashed line in (a) at a fixed value of $J/U = 0.01$. For comparison, we also plot the same quantities of $J = 0$ in (b). The model parameters are set as $U_{aa} = U_{bb} = U$, $U_{ab}/U = 0.5$ and $W = 0$.

species particle-hole pairings are condensed [10, 12]. In terms of pseudo-spins, it can also be re-interpreted as the XY ferromagnet phase [11]. Recently, the SCF phase has been observed in experiments via probing the anti-pair correlations [18]. Theoretically, the SCF phase can be verified by $\langle a \rangle = \langle b \rangle = 0$ and $\langle ab^\dagger \rangle \neq 0$ in the single-site Gutzwiller mean-field approach (SGMF) [61, 62]. In the SCF phase, the non-zero $\langle ab^\dagger \rangle$ comes from the degenerate single-site ground states. Unfortunately, this degeneracy is easily destroyed by finite-size effects in a cluster-like mean-field method, i.e. the CGMF. This is because if $\langle a \rangle = \langle b \rangle = 0$, the CGMF Hamiltonian becomes exactly for a cluster which should be solved via the exact diagonalization (ED). In actual CGMF calculations, we find that the order parameter $\langle ab^\dagger \rangle$ is always zero for $J \neq 0$ within the SCF lobes. While for $J = 0$, the CGMF back to the SGMF, and $\langle ab^\dagger \rangle$ is nonzero in an SCF state. The SCF phase boundaries evaluated by these two methods as well as the $\langle ab^\dagger \rangle$ as a function of μ are depicted in Fig. A3(a)-(b). Indeed, as shown in Fig. A3(b), one can see that $\langle ab^\dagger \rangle$, calculated by the CGMF approach, is zero at $J/U = 0.01$ and is non-zero at $J = 0$ within the SCF lobe of Fig. A3(a).

Due to this reason, the order parameter $\langle ab^\dagger \rangle$ is not suitable to distinguish the SCF phase from the MI state in CGMF theory. Instead, we introduce two other parameters: the local particle-number fluctuations Δn_α and the interspecies entanglement entropy S . In Fig. A3(b), we plot Δn_α and S v.s. μ/U for a fixed value of J/U . As it shows, both two quantities are non-zero within the SCF lobe, attributed to the compressibility and the presence of interspecies particle-hole pairing. In addition, these two quantities remain unchanged with respect to μ/U at fixed values of J within the SCF lobe owing to its cluster ground state being independent of μ/U in this situation. In formalism, it is $(\partial \Delta n_\alpha / \partial \mu)_J = (\partial S / \partial \mu)_J = 0$, which can be applied to find out the SCF-2SF phase boundary. This boundary matches the boundary presented in Fig. A3(a) where the SCF-2SF critical values are located by $\langle a \rangle = \langle b \rangle = 0$. Hence, all the SCF and SCF-like phase boundaries in this paper are determined through $\langle a \rangle = \langle b \rangle = 0$ for convenience. Although $\langle ab^\dagger \rangle_{J=0} \neq 0$ and $\langle ab^\dagger \rangle_{J \neq 0} = 0$ in the cluster SCF ground state, we clarify that the whole region enclosed by the SCF phase boundaries have the same physical properties. The main reason is that the SCF lobes obtained by the CGMF and SGMF are overlapped, while in SGMF, $\langle ab^\dagger \rangle$ is non-zero in the entire SCF lobe.

Appendix C: The impact of the interspecies interaction U_{ab} on the phase diagrams

Here, we will analyze the influence of the interspecies interaction U_{ab} on the phase diagrams of the two-component bosonic systems with SPH interaction. We are only interested in the phase diagrams with integer total filling. If the total filling $f = \langle n_a \rangle + \langle n_b \rangle$ equals 1, it is easy to know that only the SCF state can be the ground state and the corresponding eigenvalue is $-\mu$. However, three possible states, i.e., PSCF, 2MI, and SCF*, can be the ground state of the $f = 2$ lobe in the ground-state phase diagram. Which of these three possible phases is the truly ground state depends on the strength of the interspecies interaction U_{ab} . Numerical results can be found in Fig. A4.

Let us consider the case at atomic limit $J = 0$ first. In this situation, the whole ground state can be decoupled as the product of the single-site wave functions, that is $|\Psi\rangle = \otimes_i |\Psi_i\rangle$. Therefore, below we can only analyze the ground state of the Hamiltonian on a single site. If the ground state of the $f = 2$ lobe is the PSCF phase, the corresponding eigenstate can be assumed as,

$$|\Psi_{\text{PSCF}}\rangle = \beta(k|2, 0\rangle + |0, 2\rangle), \quad (\text{C1})$$

where we have $\beta^2 = 1/(k^2 + 1)$. With the help of the fact $U_{aa}/2n_a(n_a - 1)|\Psi_{\text{PSCF}}\rangle = U_{aa}\beta k|2, 0\rangle$, $U_{bb}/2n_b(n_b - 1)|\Psi_{\text{PSCF}}\rangle = U_{bb}\beta|0, 2\rangle$, $U_{ab}n_a n_b|\Psi_{\text{PSCF}}\rangle = 0$, $-\mu(n_a + n_b)|\Psi_{\text{PSCF}}\rangle = -2\mu|\Psi_{\text{PSCF}}\rangle$, and $W(\hat{a}^\dagger \hat{a}^\dagger \hat{b} \hat{b} + \text{H.c.})|\Psi_{\text{PSCF}}\rangle = 2W\beta(|2, 0\rangle + k|0, 2\rangle)$, we can obtain $H|\Psi_{\text{PSCF}}\rangle = \beta[(U_{aa}k + 2W - 2\mu k)|2, 0\rangle + (U_{bb} + 2Wk -$

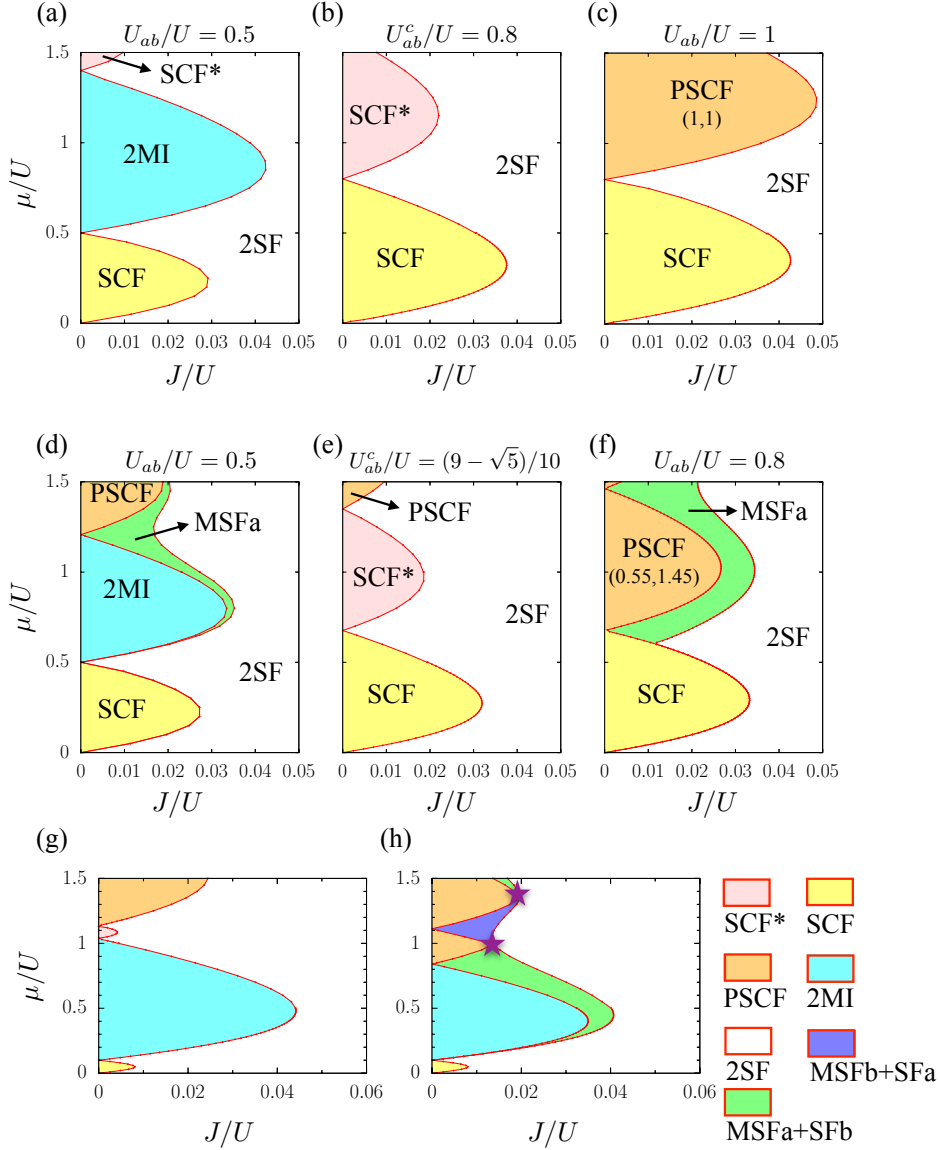


FIG. A4. (Color online) (a)-(c) The interexchange symmetric, and (d)-(f) interexchange asymmetric phase diagrams for several values of U_{ab} . Here, $U_{aa} = U_{bb} = U$ and $U_{bb} = 0.8U_{aa} = 0.8U$ is set in (a)-(c) and (d)-(f) respectively, W is fixed at $-0.1U$ in all these calculations. The critical value is $U_{ab}^c = U_{bb} + 2Wk$, where $k = (U_{aa} - U_{bb})/4W + [(U_{aa} - U_{bb})^2/4W^2 + 4]^{1/2}/2$ (See details in Appendix). In the upper panel, $U_{ab}^c/U = 0.8$, and in the down panel, $U_{ab}^c/U = (9 - \sqrt{5})/10$. In (c) and (f), the two PSCF lobes both have a total averaged particle numbers $\langle n_a \rangle + \langle n_b \rangle = 2$ and can be re-interpreted as the spin-1 XY2 ferromagnet phase from the perspective of pseudo-spins. (g)-(h) are the ground-state phase diagram with interexchange symmetric $U_{aa} = U_{bb} = U$ and asymmetric $U_{bb} = 0.8U_{aa} = 0.8U$ cases respectively under a weak interspecies interaction strength $U_{ab}/U = 0.1$. The two stars in (h) label the two quadruple critical points.

$2\mu|0, 2\rangle$. Since the $|\Psi_{\text{PSCF}}\rangle$ has been taken the form of Eq. (C1), the coefficients before the Fock states $|2, 0\rangle$ and $|0, 2\rangle$ should thus satisfy the relation,

$$(U_{aa}k + 2W - 2\mu k)/(U_{bb} + 2Wk - 2\mu) = k. \quad (\text{C2})$$

And then we have $H|\Psi_{\text{PSCF}}\rangle = (U_{bb} + 2Wk - 2\mu)|\Psi_{\text{PSCF}}\rangle$, and the associated energy is

$$E_{\text{PSCF}} = U_{bb} + 2Wk - 2\mu. \quad (\text{C3})$$

The Eq. (C2) can be simplified as $2Wk^2 + (U_{bb} - U_{aa})k - 2W = 0$, and we can easily obtain the solution of this equation

$$k = \frac{U_{aa} - U_{bb}}{4W} \pm \frac{1}{2} \sqrt{\frac{(U_{bb} - U_{aa})^2}{4W^2} + 4}. \quad (\text{C4})$$

While if the ground state is a 2MI state with $f = 2$, the corresponding wavefunction can be easily written as

$|\Psi_{\text{MI}}\rangle = |1, 1\rangle$ and the corresponding eigenvalue is

$$E_{\text{MI}} = U_{ab} - 2\mu. \quad (\text{C5})$$

We can now analyze the ground state of the $f = 2$ lobe by comparing the energies of the 2MI and the PSCF phase. If $E_{\text{MI}} < E_{\text{PSCF}}$, the ground state is a 2MI state, otherwise, the ground state is a PSCF state. The critical point is thus,

$$U_{ab}^c = U_{bb} + 2Wk. \quad (\text{C6})$$

At U_{ab}^c , the ground state is a SCF* state because the ground state is a combination of $|\Psi_{\text{PSCF}}\rangle$ and $|\Psi_{2\text{MI}}\rangle$.

It can be read as $|\Psi_{\text{SCF}^*}\rangle = \beta(k|2, 0\rangle + |0, 2\rangle) + \gamma|1, 1\rangle$, where γ is a unknown parameter. Note that in $|\Psi_{\text{SCF}^*}\rangle$, it is clear that the order parameters $\langle ab^\dagger \rangle$ and $\langle (ab^\dagger)^2 \rangle$ are both nonzero. In particular, if we chose $U_{aa} = 1$, $U_{bb} = 0.8$ and $W = -0.1$, the value of k is equal to 0.618034 or -1.61803 . But the negative values of k need to be discarded since $E_{\text{PSCF}}^{k < 0} > E_{\text{PSCF}}^{k > 0}$ for $W < 0$. Hence, the related value of U_{ab}^c under these settings equals $(9 - \sqrt{5})/10$. This exactly matches the numerical calculations in the main text.

Similarly, these analyses can be applied to the first SCF lobe with $f = 1$ for the atomic limit $J = 0$. By setting $E_{\text{SCF}} \leq E_{\text{MI}}$ and $E_{\text{SCF}} \leq E_{\text{PSCF}}$, we find that the chemical potential width of the first SCF lobe at $J = 0$ is U_{ab} and U_{ab}^c respectively when $U_{ab} < U_{ab}^c$ and $U_{ab} > U_{ab}^c$.

-
- [1] F. Dalfovo, S. Giorgini, L. P. Pitaevskii, and S. Stringari, *Rev. Mod. Phys.* **71**, 463 (1999).
- [2] M. Lewenstein, A. Sanpera, V. Ahufinger, B. Damski, A. Sen(De), and U. Sen, *Advances in Physics* **56**, 243 (2007).
- [3] M. Lewenstein, A. Sanpera, and V. Ahufinger, *Ultracold Atoms in Optical Lattices: Simulating quantum many-body systems* (Oxford University Press, 2012).
- [4] T. Sowiński and M. A. García-March, *Rep. Prog. Phys.* **82**, 104401 (2019).
- [5] M. Greiner, O. Mandel, T. Esslinger, T. W. Hänsch, and I. Bloch, *Nature* **415**, 39 (2002).
- [6] L. Tanzi, E. Lucioni, F. Famà, J. Catani, A. Fioretti, C. Gabbanini, R. N. Bisset, L. Santos, and G. Modugno, *Phys. Rev. Lett.* **122**, 130405 (2019).
- [7] F. Böttcher, J.-N. Schmidt, M. Wenzel, J. Hertkorn, M. Guo, T. Langen, and T. Pfau, *Phys. Rev. X* **9**, 011051 (2019).
- [8] L. Chomaz, D. Petter, P. Ilzhöfer, G. Natale, A. Trautmann, C. Politi, G. Durastante, R. M. W. van Bijnen, A. Patscheider, M. Sohmen, M. J. Mark, and F. Ferlaino, *Phys. Rev. X* **9**, 021012 (2019).
- [9] F. Böttcher, J.-N. Schmidt, J. Hertkorn, K. S. H. Ng, S. D. Graham, M. Guo, T. Langen, and T. Pfau, *Rep. Prog. Phys.* **84**, 012403 (2020).
- [10] A. B. Kuklov and B. V. Svistunov, *Phys. Rev. Lett.* **90**, 100401 (2003).
- [11] E. Altman, W. Hofstetter, E. Demler, and M. D. Lukin, *New J. Phys.* **5**, 113 (2003).
- [12] A. Kuklov, N. Prokof'ev, and B. Svistunov, *Phys. Rev. Lett.* **92**, 050402 (2004).
- [13] O. Mandel, M. Greiner, A. Widera, T. Rom, T. W. Hänsch, and I. Bloch, *Nature* **425**, 937 (2003).
- [14] J. Catani, L. De Sarlo, G. Barontini, F. Minardi, and M. Inguscio, *Phys. Rev. A* **77**, 011603 (2008).
- [15] P. N. Jepsen, J. Amato-Grill, I. Dimitrova, W. W. Ho, E. Demler, and W. Ketterle, *Nature* **588**, 403 (2020).
- [16] W. C. Chung, J. de Hond, J. Xiang, E. Cruz-Colón, and W. Ketterle, *Phys. Rev. Lett.* **126**, 163203 (2021).
- [17] J. de Hond, J. Xiang, W. C. Chung, E. Cruz-Colón, W. Chen, W. C. Burton, C. J. Kennedy, and W. Ketterle, *Phys. Rev. Lett.* **128**, 093401 (2022).
- [18] Y.-G. Zheng, A. Luo, Y.-C. Shen, M.-G. He, Z.-H. Zhu, Y. Liu, W.-Y. Zhang, H. Sun, Y. Deng, Z.-S. Yuan, and J.-W. Pan, *Nature Physics* (2025), 10.1038/s41567-024-02732-5.
- [19] A. Argüelles and L. Santos, *Phys. Rev. A* **75**, 053613 (2007).
- [20] E. K. Dahl, E. Babaev, and A. Sudbø, *Phys. Rev. Lett.* **101**, 255301 (2008).
- [21] Ş. G. Söyler, B. Capogrosso-Sansone, N. V. Prokof'ev, and B. V. Svistunov, *New J. Phys.* **11**, 073036 (2009).
- [22] A. Hubener, M. Snoek, and W. Hofstetter, *Phys. Rev. B* **80**, 245109 (2009).
- [23] L. Mathey, I. Danshita, and C. W. Clark, *Phys. Rev. A* **79**, 011602 (2009).
- [24] A. Hu, L. Mathey, I. Danshita, E. Tiesinga, C. J. Williams, and C. W. Clark, *Phys. Rev. A* **80**, 023619 (2009).
- [25] C. Menotti and S. Stringari, *Phys. Rev. A* **81**, 045604 (2010).
- [26] Z. Lin, C. Liu, and Y. Chen, *Phys. Rev. Lett.* **125**, 245301 (2020).
- [27] H. J. Schulz, *Phys. Rev. B* **34**, 6372 (1986).
- [28] O. Boada, A. Celi, J. I. Latorre, and M. Lewenstein, *Phys. Rev. Lett.* **108**, 133001 (2012).
- [29] T. Ozawa and H. M. Price, *Nat. Rev. Phys.* **1**, 349 (2019).
- [30] A. Celi, P. Massignan, J. Ruseckas, N. Goldman, I. B. Spielman, G. Juzeliūnas, and M. Lewenstein, *Phys. Rev. Lett.* **112**, 043001 (2014).
- [31] F. Schäfer, T. Fukuhara, S. Sugawa, Y. Takasu, and Y. Takahashi, *Nat. Rev. Phys.* **2**, 411 (2020).
- [32] T. Keilmann, S. Lanzmich, I. McCulloch, and M. Roncaglia, *Nat. Commun.* **2**, 361 (2011).
- [33] A. Rapp, X. Deng, and L. Santos, *Phys. Rev. Lett.* **109**, 203005 (2012).
- [34] S. Greschner, L. Santos, and D. Poletti, *Phys. Rev. Lett.* **113**, 183002 (2014).
- [35] C. Sträter, S. C. L. Srivastava, and A. Eckardt, *Phys. Rev. Lett.* **117**, 205303 (2016).
- [36] F. Meinert, M. J. Mark, K. Lauber, A. J. Daley, and H.-C. Nägerl, *Phys. Rev. Lett.* **116**, 205301 (2016).
- [37] L. W. Clark, B. M. Anderson, L. Feng, A. Gaj, K. Levin, and C. Chin, *Phys. Rev. Lett.* **121**, 030402 (2018).
- [38] L. D. Marin Bukov and A. Polkovnikov, *Advances in Physics* **64**, 139 (2015).

- [39] N. Goldman and J. Dalibard, *Phys. Rev. X* **4**, 031027 (2014).
- [40] A. Eckardt, *Rev. Mod. Phys.* **89**, 011004 (2017).
- [41] C. Weitenberg and J. Simonet, *Nature Physics* **17**, 1342 (2021).
- [42] M. Iskin, *Phys. Rev. A* **82**, 033630 (2010).
- [43] T. Mishra, R. V. Pai, and B. P. Das, *Phys. Rev. A* **76**, 013604 (2007).
- [44] T. Ozaki and T. Nikuni, *J. Phys. Soc. Jpn.* **81**, 024001 (2012).
- [45] F. Zhan and I. P. McCulloch, *Phys. Rev. A* **89**, 057601 (2014).
- [46] F. Lingua, M. Guglielmino, V. Penna, and B. Capogrosso Sansone, *Phys. Rev. A* **92**, 053610 (2015).
- [47] Q. Zhou, J. V. Porto, and S. Das Sarma, *Phys. Rev. B* **83**, 195106 (2011).
- [48] F. Pinheiro, G. M. Bruun, J.-P. Martikainen, and J. Larson, *Phys. Rev. Lett.* **111**, 205302 (2013).
- [49] E. Altman, W. Hofstetter, E. Demler, and M. D. Lukin, *New J. Phys.* **5**, 113 (2003).
- [50] A. Hu, L. Mathey, C. J. Williams, and C. W. Clark, *Phys. Rev. A* **81**, 063602 (2010).
- [51] M. Fishman, S. R. White, and E. M. Stoudenmire, *SciPost Phys. Codebases*, 4 (2022).
- [52] A. Marte, T. Volz, J. Schuster, S. Dürr, G. Rempe, E. G. M. van Kempen, and B. J. Verhaar, *Phys. Rev. Lett.* **89**, 283202 (2002).
- [53] L.-M. Duan, E. Demler, and M. D. Lukin, *Phys. Rev. Lett.* **91**, 090402 (2003).
- [54] D. Pekker, B. Wunsch, T. Kitagawa, E. Manousakis, A. S. Sørensen, and E. Demler, *Phys. Rev. B* **86**, 144527 (2012).
- [55] D.-S. Lühmann, *Phys. Rev. A* **87**, 043619 (2013).
- [56] B. K. Alavani, A. Das, and R. V. Pai, *J. Phys. B: At. Mol. Opt. Phys.* **51**, 145302 (2018).
- [57] P. Chen and C. Liu, *Phys. Lett. A* **507**, 129485 (2024).
- [58] R. Kraus, K. Biedroń, J. Zakrzewski, and G. Morigi, *Phys. Rev. B* **101**, 174505 (2020).
- [59] F. Cartarius, A. Minguzzi, and G. Morigi, *Phys. Rev. A* **95**, 063603 (2017).
- [60] B.-L. Chen, S.-P. Kou, Y. Zhang, and S. Chen, *Phys. Rev. A* **81**, 053608 (2010).
- [61] V. E. Colussi, F. Caleffi, C. Menotti, and A. Recati, *SciPost Phys.* **12**, 111 (2022).
- [62] C. Liu, P. Chen, L. He, and F. Xu, *Phys. Rev. A* **108**, 013309 (2023).
- [63] I. Bloch, J. Dalibard, and W. Zwerger, *Rev. Mod. Phys.* **80**, 885 (2008).